

Supporting Information

Sensory gating in bilayer amorphous carbon memristors

T J Raeber¹, A J Barlow², Z C Zhao³, D R McKenzie³, J G Partridge¹, D G McCulloch¹, B J Murdoch^{*1}

¹School of Science, RMIT University, VIC 3001, Melbourne, Australia

²Centre for Materials and Surface Science (CMSS), Department of Chemistry and Physics, La Trobe University, VIC 3086, Melbourne, Australia

³School of Physics, The University of Sydney, NSW 2006, Sydney, Australia

*Corresponding author (BJM) : billy.murdoch@rmit.edu.au

Supplementary Note 1

Detailed experimental methods

1. Filtered cathodic vacuum arc (FCVA) deposition

Layers of a-CO_x/ta-C were deposited in a NanoFilm FCVA using a 68mm graphitic carbon cathode. The substrates were mounted on a temperature controlled stage, which was heated to 100°C prior to deposition. Thermal contact was made to the surface of the substrate either via metallic clips to the bottom electrodes, in the case of through film devices, or directly via the Si wafer substrate. Wafers used for XPS and spectroscopic ellipsometry were n-type <100> silicon wafers (resistivity ~ 10 Ω.cm). Substrates for electrical devices were Si wafers with 1µm thick thermally-grown SiO₂ layers. The temperature rise due to the plasma was measured previously to be <50°C for carbon depositions¹. Energetic deposition was achieved by depositing through a carbon-coated steel mesh grid, which has previously been developed and characterised *in-house* for the purpose of ta-C deposition onto low conductivity substrates². No Fe was detected in the films by XPS or EDS. The mesh was biased to -100V. Deposition of bilayers was achieved without breaking vacuum by, firstly, depositing the oxygenated carbon films by inletting O₂ into the deposition chamber near the substrate holder for reactive depositions, then evacuating the chamber to <5 x 10⁻⁶ Torr before depositing ta-C layers.

2. X-ray photoelectron spectroscopy (XPS)

Chemical analysis of single layer a-CO_x deposited onto Si wafers was performed using XPS. The instrument used was a Kratos AXIS Nova with monochromated Al 1487 eV K-α source. Charge compensation using a flood gun was not required. Peak fitting was performed using the Thermo Scientific Avantage XPS software package. The background signal subtraction of the C1s peak region of each sample was removed using a Shirley background model. The ta-C film was assumed to consist of 2 peaks – an asymmetric C-C *sp*² peak at 284 eV, which was fit with a convolution of a Gaussian-Lorentzian function peak with asymmetric broadening on the high binding energy side, and a symmetric C-C *sp*³ peak at 284.8 eV, which was fit with a symmetric convolution of a Gaussian-Lorentzian peak. The asymmetric broadening in the *sp*² peak was kept constant and used for peak fitting of the more complex oxygenated a-C samples, which included symmetric convolutions of Gaussian-Lorentzian C-O-C (286 eV) and O-C=O (288.5 eV) peaks. As quantification of the *sp*²/*sp*³ fraction by peak fitting the C1s region from carbon samples by XPS is often impossible, we used EELS to verify the *sp*² fraction of these samples. For ta-C, EELS and XPS indicated *sp*² fractions of 37.2% and 37.5%, respectively. For a-CO_x deposited at an O₂ partial pressure of 0.5 mTorr, EELS and XPS indicated *sp*² fractions of 53.5% and 56.5%, respectively.

3. Spectroscopic ellipsometry

Variable angle spectroscopic ellipsometry was performed using a JA Woollam Co. M-2000. The ψ and Δ parameters were collected in the range 190-1000 nm at 65°, 70° and 75° angles. The real (ε₁) and imaginary (ε₂)

dielectric functions and thickness were calculated by using a general oscillator model. The thickness was verified using scanning profilometry measurements over a step-edge in the film. The optical band gap was calculated using the method of Tauc³. A linear fit to E vs. $E\sqrt{\epsilon_2}$ yielded the optical band gap values. These plots were found to produce equivalent optical band gap values to E vs. $(\alpha E)^{1/2}$ (where the absorption coefficient $\alpha = 4\pi\kappa/\lambda$), indicating an indirect band gap.

4. Transmission electron microscopy (TEM)

TEM was performed in a JEOL 2100F operating at an accelerating voltage of 80kV, which is below the threshold displacement energy for graphitic carbon⁴. Scanning transmission electron microscope (STEM) images were obtained in high angle annular dark field (HAADF) mode with convergence semi-angle $\alpha = 9.57$ mrad and collection semi-angle $\beta = 6.69$ mrad. A cross-sectioned TEM lamella was prepared using the lift-out technique in dual-beam FEI Scios focused ion beam (FIB) system.

5. Electron energy loss spectroscopy (EELS)

EELS was performed using a Gatan imaging filter (GIF) fitted to the Jeol 2100f. Images were collected in STEM-HAADF mode. The maximum resolution of the spectrometer, as indicated by the FWHM of the zero-loss peak was 0.7 eV. C-C sp^2 fractions for the sample were extracted from C K edge core-loss spectra⁵. The low loss EELS spectra were used to estimate the density of the samples by assuming a free electron model⁶. Four valence electrons were assumed for each atom in the ta-C layer (consisting of pure carbon). An average valence electron density of 4.26 was calculated for the a-CO_x layer (deposited at 0.5 mTorr), which was measured to be 13 at% O and 87 at% C by EDS, assuming 4 valence electrons for C atoms and 6 valence electrons for O atoms. The molecular mass was determined to be 12.52 g/mol.

6. Electrical measurements

I - V characteristics were analysed using a programmable Keysight B2900A source-measure unit in air using tungsten needle probes. Zero bias capacitance measurements were made using a Boonton 7200 capacitance meter. I - V characteristics were modelled using a Schottky emission model. The barrier height (ϕ_B) and optical frequency dielectric constant (ϵ_1) were extracted using a linear fit to $\ln(J/T^2)$ vs. \sqrt{E} , as per the method outlined in⁷. The effective mass of an electron in carbon was assumed to be $0.87m_e$ ⁸.

7. Conductive atomic force microscopy (C-AFM)

C-AFM experiments were performed using an Asylum Research MFP 3D AFM in contact mode. Conductive PtIr coated Si tips with a force constant of 42 N/m and tip radius of 25 ± 5 nm were used. DC voltages were applied to the bottom Ag electrode (as with the lithographically defined devices) with the tip grounded.

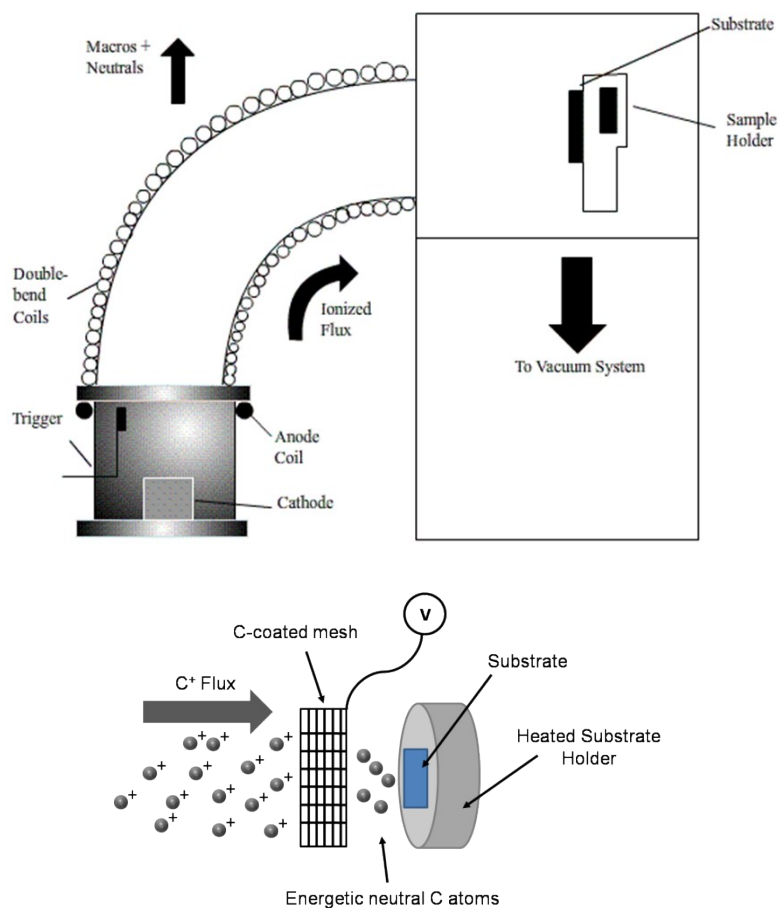


Figure S1. Schematic diagrams of FCVA deposition system and biased mesh apparatus for deposition of energetic neutral atoms.

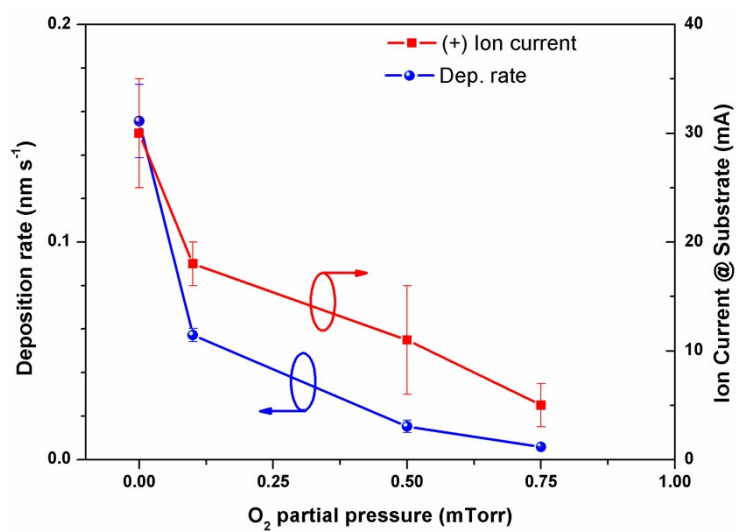


Figure S2. Deposition rate and positive ion current at the substrate measured during filtered cathodic vacuum arc (FCVA) deposition of a-CO_x films in O₂ atmospheres. The ion current and deposition rate are both reduced proportionally as the pressure is increased. The film growth is inhibited by scattering of the depositing ions rather than due to sputtering at the substrate.

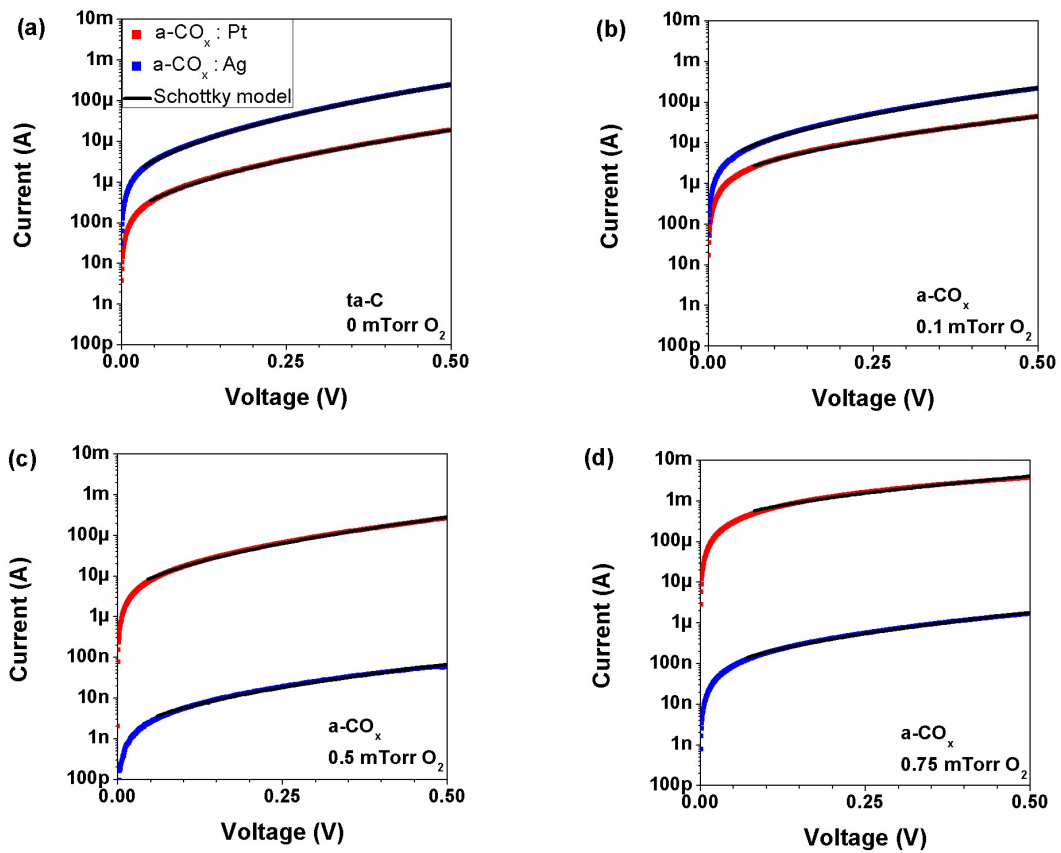


Figure S3. Schottky emission model fitting to I - V curves fitting of the $a\text{-CO}_x$ films deposited at O_2 partial pressures of (a) 0 mTorr, (b) 0.1 mTorr, (c) 0.5 mTorr and (d) 0.75 mTorr contacted by Pt (blue) and Ag (red).

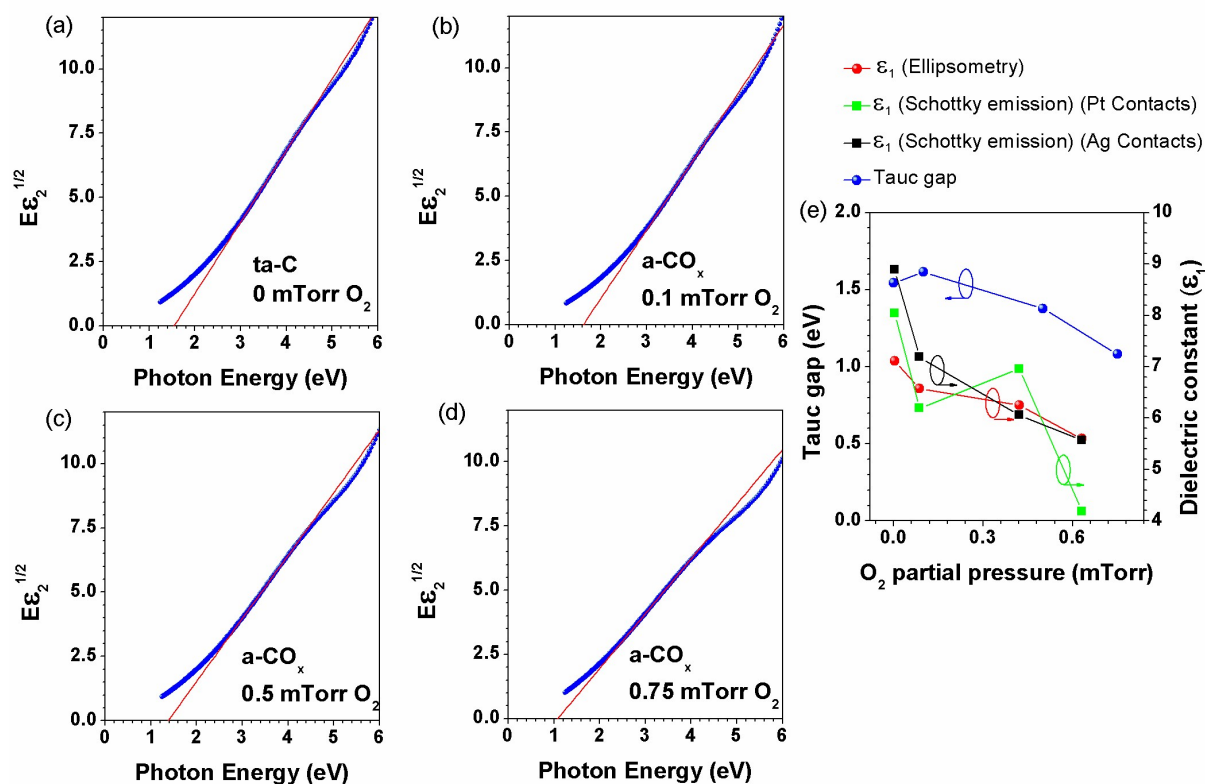


Figure S4. Optical properties of a- CO_x films determined by spectroscopic ellipsometry. (a-d) Tauc plots constructed from the imaginary component of the dielectric function, ϵ_2 . (e) Optical (Tauc) band gap and real dielectric constant measured at 633nm as a function of oxygen partial pressure. The dielectric constants extracted from Schottky emission plots (Supplementary Fig. S2) are also shown for comparison.

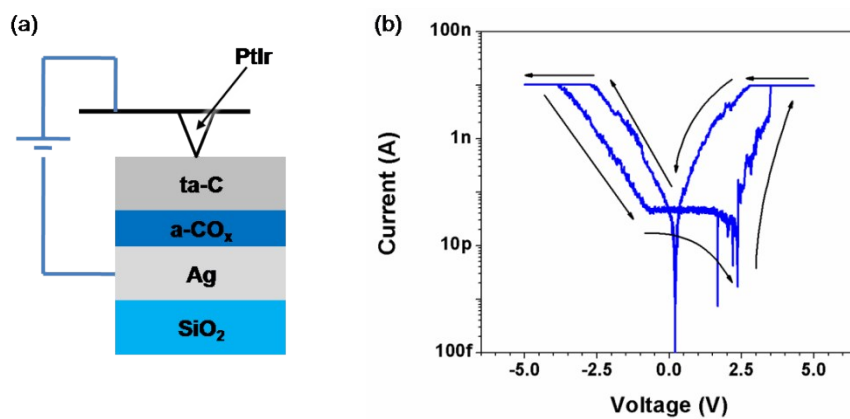


Figure S5. (a) Schematic diagram of the C-AFM experiment performed with a PtIr-coated tip of nominal radius 25 ± 5 nm. The root mean square roughness of the device (without the Pt top electrode) was determined to be <0.5 nm. (b) I-V curves obtained from the C-AFM experiments showing reversible bipolar resistive switching on the nanoscale.

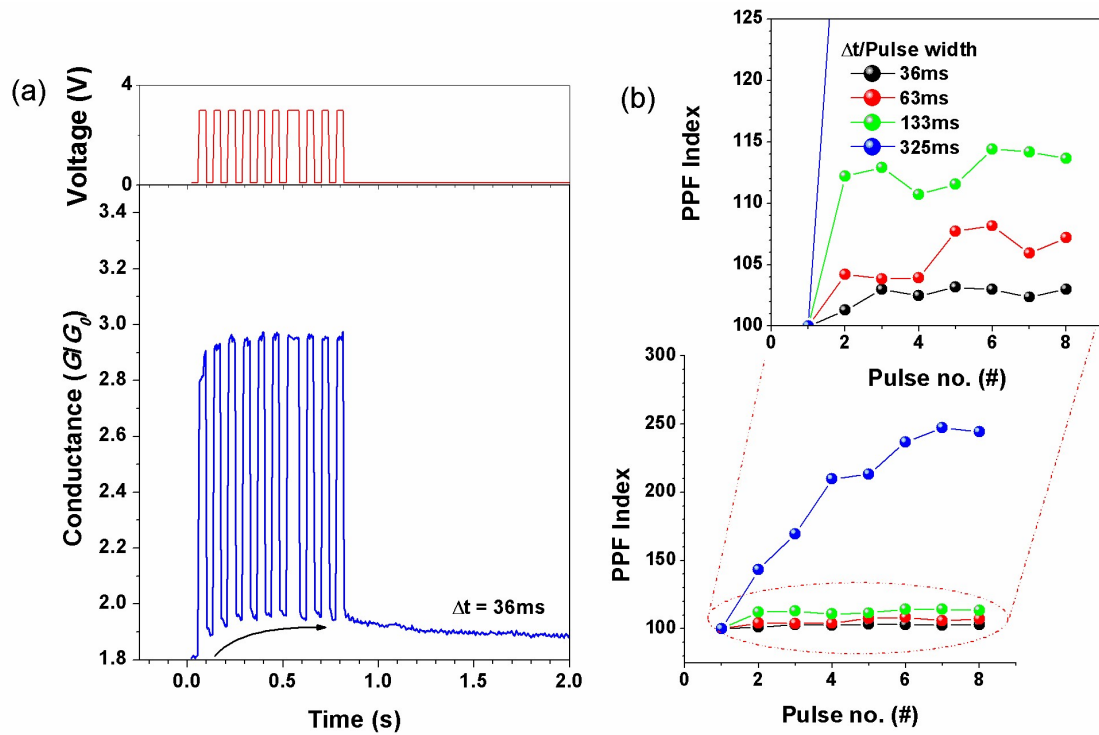


Figure S6. (a) Paired-pulse facilitation (PPF) in response to a voltage-pulse train is observed when the post-(1st)pulse conductance is low ($<5 G_0$). (b) PPF in response to voltage pulse trains (3V) at time interval Δt . Note, the pulse width during this experiment was made equivalent to Δt . The increase in PPF is due to the increase in pulse width.

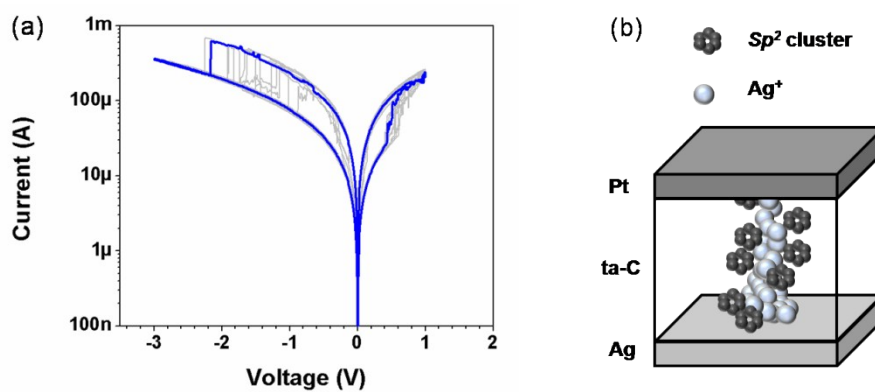


Figure S7. (a) I - V measurements during 10x bipolar switching cycles for a single-layer Ag/ta-C/Pt device. (b) Schematic diagram of the single layer device.

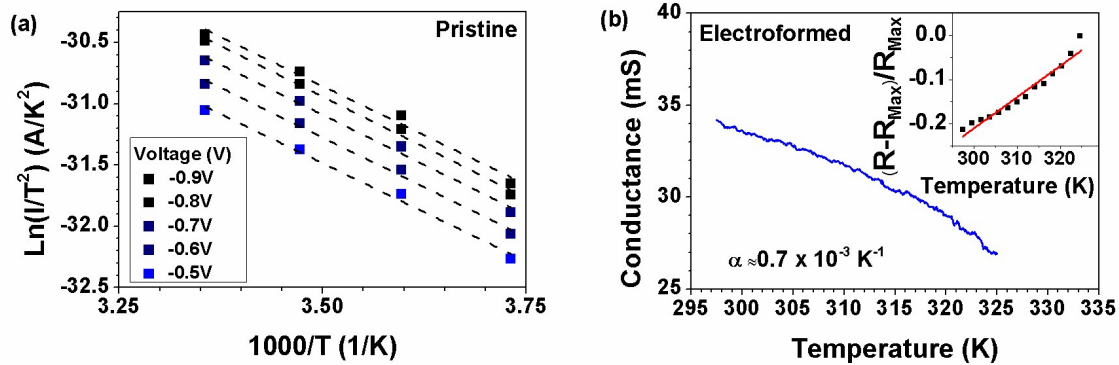


Figure S8. (a) Richardson plot of the Ag/a-CO_x/ta-C/Pt memristors showing thermionic emission in their pristine state. The reverse bias characteristics were analysed to reduce the likelihood of electroforming. (b) Conductance – temperature characteristics for the memristors in the fully-electroformed state (measured at 1 mA after electroforming with a 1 mA current compliance at ~4V). Inset shows a plot of $(R-R_{\text{Max}})/R_{\text{Max}}$ vs. temperature, which was used to extract the temperature coefficient of resistance (α). The calculated temperature coefficient is $\alpha = 0.7 \times 10^{-3} \text{ K}^{-1}$, which is close to the value reported for Ag nanowires (defect-free Ag nanowires are $\sim 2.5 \times 10^{-3} \text{ K}^{-1}$)⁹. Note that reported α values are typically lower for Ag filaments embedded in dielectric layers^{10, 11}.

References

1. Lau, D. W. M.; Moafi, A.; Taylor, M. B.; Partridge, J. G.; McCulloch, D. G.; Powles, R. C.; McKenzie, D. R. The structural phases of non-crystalline carbon prepared by physical vapour deposition *Carbon* **2009**, 47, (14), 3263-3270.
2. Moafi, A.; Lau, D. W. M.; Sadek, A. Z.; Partridge, J. G.; McKenzie, D. R.; McCulloch, D. G. Energetic deposition of carbon in a cathodic vacuum arc with a biased mesh *Journal of Applied Physics* **2011**, 109, (7), 073309.
3. Tauc, J. Optical properties and electronic structure of amorphous Ge and Si *Materials Research Bulletin* **1968**, 3, (1), 37-46.
4. Egerton, R.; Li, P.; Malac, M. Radiation damage in the TEM and SEM *Micron* **2004**, 35, (6), 399-409.
5. Berger, S. D.; McKenzie, D. R.; Martin, P. J. EELS analysis of vacuum arc-deposited diamond-like films *Philosophical Magazine Letters* **1988**, 57, (6), 285-290.
6. Egerton, R. F., *Electron Energy-Loss Spectroscopy in the Electron Microscope*. Plenum Press: 1996.
7. Jones, M.; Kwon, Y.; Norton, D. Dielectric constant and current transport for HfO₂ thin films on ITO *Appl. Phys. A* **2005**, 81, (2), 285-288.
8. LiBassi, A.; Ferrari, A.; Stolojan, V.; Tanner, B.; Robertson, J.; Brown, L. Density, sp³ content and internal layering of DLC films by X-ray reflectivity and electron energy loss spectroscopy *Diamond and Related Materials* **2000**, 9, (3-6), 771-776.
9. Bid, A.; Bora, A.; Raychaudhuri, A. Temperature dependence of the resistance of metallic nanowires of diameter ≥ 15 nm: Applicability of Bloch-Grüneisen theorem *Physical Review B* **2006**, 74, (3), 035426.
10. Yoon, J. H.; Wang, Z.; Kim, K. M.; Wu, H.; Ravichandran, V.; Xia, Q.; Hwang, C. S.; Yang, J. J. An artificial nociceptor based on a diffusive memristor *Nature communications* **2018**, 9, (1), 417.
11. Murdoch, B. J.; Raeber, T. J.; Barlow, A. J.; McCulloch, D. G.; Partridge, J. G. Non-volatile and volatile memory behaviour in oxygenated amorphous carbon electrochemical metallisation devices *Applied Physics Letters* **2018**, 112, (24), 242903.